Nuclear Engineering and Technology 52 (2020) 1355–1366

Contents lists available at ScienceDirect

Nuclear Engineering and Technology

journal homepage: www.elsevier.com/locate/net

Original Article

Interpretation of two SINBAD photon-leakage benchmarks with nuclear library ENDF/B-VIII.0 and Monte Carlo code MCS

Matthieu Lemaire, Hyunsuk Lee, Peng Zhang, Deokjung Lee*

Department of Nuclear Engineering, Ulsan National Institute of Science and Technology, 50, UNIST-gil, Ulsan, 44919, Republic of Korea

ARTICLE INFO

Article history:
Received 4 June 2019
Received in revised form
18 November 2019
Accepted 13 December 2019
Available online 19 December 2019

Keywords:
ENDF/B-VIII.0
Gamma production
SINBAD shielding benchmark
14 MeV neutron source
Monte Carlo interpretation

ABSTRACT

A review of the documentation and an interpretation of the NEA-1517/74 and NEA-1517/80 shielding benchmarks (measurements of photon leakage flux from a hollow sphere with a central 14 MeV neutron source) from the SINBAD database with the Monte Carlo code MCS and the most up-to-date ENDF/B-VIII.0 neutron data library are conducted. The two analyzed benchmarks describe satisfactorily the energy resolution of the photon detector and the geometry of the spherical samples with inner beam tube, tritium target and cooling water circuit, but lack information regarding the detector geometry and the distances of shields and collimators relatively to the neutron source and the detector. Calculations are therefore conducted for a sphere model only. A preliminary verification of MCS neutron-photon calculations against MCNP6.2 is first conducted, then the impact of modelling the inner beam tube, tritium target and cooling water circuit is assessed. Finally, a comparison of calculated results with the libraries ENDF/B-VII.1 and ENDF/B-VIII.0 against the measurements is conducted and shows reasonable agreement. The MCS and MCNP inputs used for the interpretation are available as supplementary material of this article.

1. Introduction

This paper presents a review and interpretation with the most up-to-date neutron data library ENDF/B-VIII.0 [1] of reactor shielding experiments known as NEA-1517/74 and NEA-1517/80 in the Shielding Integral Benchmark Archive and Database (SINBAD) [2]. The SINBAD database is maintained jointly by the Radiation Safety Information Computational Center (RSICC) and the Nuclear Energy Agency (NEA) Data Bank. It contains compilations and evaluations of over 100 shielding benchmarks and is widely used for computer code and neutron/gamma nuclear data validation [3].

The NEA-1517/74 [4] and NEA-1517/80 [5] experiments, released in SINBAD from 2005, were conducted at the Russian Federal Nuclear Center (RFNC) in Snezhinsk and deal with the measurements of photon leakage from hollow spherical samples with a central 14 MeV neutron source produced by deuterium-tritium (D-T) fusion. Measurements for seven (Al, Ti, Fe, Cu, Zr, Pb and ^{238}U) and three (H_2O, NaCl, SiO_2) sphere materials are available respectively in the NEA-1517/74 and NEA-1517/80 experiments, for the purpose of the validation of neutron-transport data, gamma-production data from neutron interactions and photon-transport data. The benchmark data is of special interest for fusion applications as the accurate determination of dose due to the gammas generated by 14 MeV D-T neutrons is an important challenge of fusion devices [6]. From a broader point of view, accurate gamma flux and corresponding values of photon KERMA (Kinetic Energy Released per MAss) are crucial for the thermal studies and material strength studies of material-testing reactors [7,8] and fast reactors [9] and for the determination of hot spots in the pin power map of light-water reactors [10].

Investigation of the literature reveals that the first interpretation of the photon leakage measurements for the ten sphere materials was conducted in 2004 by the RFNC benchmark authors with the MCNP.4a code and the neutron-data libraries ENDL-92, ENDF/B-V and ENDF/B-VI [11]. Significant discrepancies between calculated and experimental photon spectra were observed and recommendations to correct the nuclear data were established. A second interpretation was conducted in 2017 for the iron sphere and water sphere only to test the available photo-atomic data libraries for fusion applications [12]. The two cases were calculated

* Corresponding author. Department of Nuclear Engineering, Ulsan National Institute of Science and Technology, Bldg. 112, Room 501-6, 50 UNIST-gil, Ulsan, 44919, Republic of Korea.
E-mail addresses: mlemaire@unist.ac.kr (M. Lemaire), hyunsuklee@unist.ac.kr (H. Lee), zhangpeng@unist.ac.kr (P. Zhang), deokjung@unist.ac.kr (D. Lee).

https://doi.org/10.1016/j.net.2019.12.014

with the MCNP6 code, the neutron-data library ENDF/B-VII.1 and the photon-atomic libraries 04p, 84p and 12p from the MCNP code package. A good consistency was observed between measured and calculated photon spectra and no significant difference was observed between the calculations with the three tested photo-atomic libraries. The most recent interpretation was conducted in 2018 for five sphere materials (Al, Cu, Zr, Pb and water spheres) with the Monte Carlo code McCARD and the neutron-data libraries ENDF/B-VII.0, ENDF/B-VII.1 and JENDL-4.0 [13]. The calculated photon spectra from the three libraries were shown to be similar and consistent with the measured spectra. In conclusion of this literature survey, a full interpretation of the RFNC photon leakage measurements (all the ten sphere materials) is yet to be conducted with the most up-to-date nuclear data library ENDF/B-VIII.0. This paper aims at conducting exactly this review and interpretation to provide additional validation of the ENDF/B-VIII.0 library and feedback to the evaluators regarding the gamma-production data of the ENDF/B-VIII.0 library.

The plan of this study is as follows. The calculation tools (MCS Monte Carlo code, ENDF/B-VIII.0 & EPICS2014 nuclear data library) used for the interpretation are first presented. The NEA-1517/74 and NEA-1517/80 experiments are described and a review of the options to model those experiments is provided. Further, the results are presented and include a code-to-code comparison to verify the photon flux calculation of MCS in coupled neutron-photon transport mode against the Monte Carlo code MCNP6.2, sensitivity studies to assess the impact of modelling choices and libraries on the calculated results, and the interpretation of the experimental data for all the ten sphere materials with the MCS code, the neutron-data library ENDF/B-VII.1 and ENDF/B-VIII.0 and the photon-data library EPICS2014. Conclusions and perspectives are finally drawn out.

2. Presentation of calculation tools

2.1. Monte Carlo code MCS

MCS is a 3D continuous-energy neutron-photon transport Monte Carlo code under development at the Ulsan National Institute of Science and Technology in South Korea since 2013. MCS allows for criticality and depletion runs (for nuclear reactor core analysis) and fixed-source runs with neutrons and/or photon sources (for shielding problems). MCS neutron transport kernel has notably been validated against ~300 ICSBEP criticality benchmarks [14] and the BEAVRS benchmark [15]. MCS photon transport kernel for shielding problems with a fixed photon source mode has been verified by comparison against the Monte Carlo code MCNP6.1 [16]. Neutron-transport data, gamma-production data and photon-transport data for MCS are based on ACE files generated with the NJOY processing code [17].

2.2. Neutron and photon data library

The evaluated nuclear reaction data library ENDF/B-VIII.0 was released in February 2018 by the Cross Section Evaluation Working Group (CSEWG) and has been previously tested against three 14-MeV neutron transmission experiments: Lawrence Livermore National Laboratory (LLNL) pulsed spheres, Fusion Neutronics Source (FNS) in Japan and the Oktavian experiments (the detailed listing of 14-MeV neutron transmission experiments against which both ENDF/B-VII.1 and B-VIII.0 libraries were tested is detailed in Ref. [18]). The interpretation of the 14-MeV neutron transmission experiments from RFNC (NEA-1517/74 & 80 benchmarks) has never been conducted to our knowledge with the ENDF/B-VIII.0 library and the interpretation results presented in the next sections will therefore provide additional validation to the ENDF/B-VIII.0 library.

For the materials of interest in the NEA-1517/74 & 80 benchmarks (i.e. Al, Ti, Fe, Cu, Zr, Pb, ^{238}U, H_2O, NaCl, SiO_2), the following changes in the ENDF/B-VIII.0 library compared to the previous ENDF/B-VII.1 library are expected to have an impact on the interpretation:

- ^{27}Al, ^{23}Na, ^{28}Si, ^{35,37}Cl: updated thermal capture gamma data (more than 100 new gamma lines added in total);
- ^{54,56,57,58}Fe, ^{63,65}Cu: updated neutron cross sections (especially capture cross sections);
- ^{238}U: new prompt fission gamma spectrum, average multiplicity and average energy.

No relevant changes are noted for the isotopes of Ti, Zr and Pb.

The photon-transport data associated with the ENDF/B-VIII.0 release is the EPICS2017 (Electron-Photon Interaction Cross Sections) library with updated binding energies (and hence updated photoelectric cross sections and coherent scattering data) compared to the previous EPICS2014 library associated with the ENDF/B-VII.1 library.

The calculations in the next sections are conducted only with the EPICS2014 photon library to isolate the effects of the change in the neutron library from ENDF/B-VII.1 to ENDF/B-VIII.0. The effect of the changes between EPICS2014 and EPICS2017 on the interpretation of the RFNC benchmark is not tested but is expected to be negligible anyway because the photon measurements of the RFNC benchmark are conducted above 0.37 MeV, well above the updated binding energies (the maximum binding energy is ~143 keV for fermium $Z = 100$). The 12p photo-atomic cross sections from MCNP package (eprdata12 file) are employed in all the calculations.

3. SINBAD NEA-1517/74 & NEA-1517/80 (RFNC) benchmarks

3.1. Description

The following technical data comes from Refs. [4,5]. The experimental layout is presented in Fig. 1. The main components are: a 14-MeV neutron source at the center of a spherical sample; a steel rod of diameter 3 cm and length 40 cm placed between the neutron source and the detector to improve the photon-to-neutron ratio at the location of the detector; a polyethylene collimator of length 60 cm and diameter 50 cm; a polyethylene (CH_2) cylinder of length 20 cm and diameter 10 cm, located at the entrance of the wall collimator to reduce the neutron background on the detector; a concrete wall with a polyethylene collimator and a lead collimator; and the detector placed in a shield of 5-cm-thick lead bricks to reduce the background of scattered photons and cosmic rays.

The spherical samples have an internal radius of 5 cm and external radius of 10 cm (geometrical tolerance ± 1 mm). Ten different spherical samples are used, with the weights of the samples given in Table 1. For the three samples made of loose materials (water H_2O, salt NaCl, sand SiO_2), a spherical iron container is used (about 0.5 mm thick, between the radii 4.95–5 cm for the inner surface and 10–10.05 cm for the outer surface). The design of the target unit (beam tube inside the spherical sample with cooling water circuit for the tritium target) is illustrated in Fig. 2. The arrangement of the layers at the end of the beam tube, in the direction of the deuteron beam, is as follows: the tritium target, which is a 0.05-mm-thick zirconium foil saturated with tritium located at the center of the sphere; a 3-mm-thick copper layer; the cooling water (thickness 1.5 mm); a 0.5-mm-thick copper layer (the geometrical tolerance of those values is ±0.1 mm). The gap between the inner and external jacket (materials 2 and 3 in Fig. 2) on the side of the beam tube is also filled with cooling water. Deuterons are accelerated by a 200-kV accelerator (deuteron current 200–500 μA) to collide with the tritium target, thus producing 14-

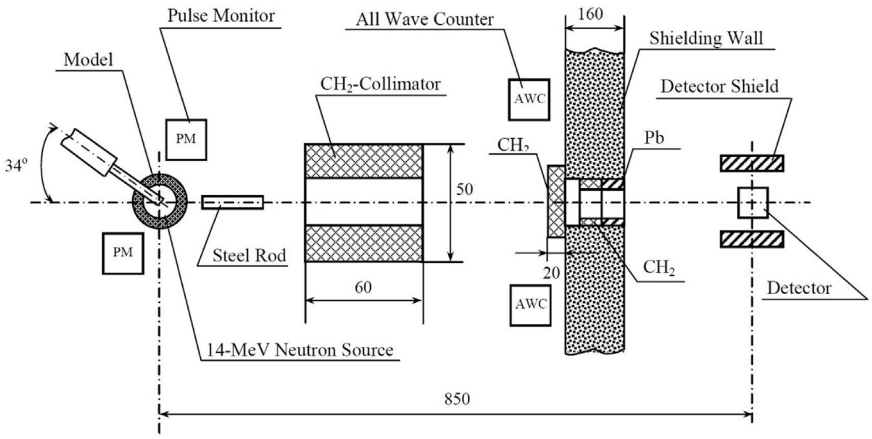

Fig. 1. Layout of RFNC 14-MeV neutron transmission experiment (dimensions in cm) [4].

Table 1
Weights of the spherical samples in kg.

Al	Ti	Fe	Cu	Zr	Pb	^{238}U	H_2O	SiO_2	NaCl
9.86	16.17	26.9	29.92	23.66	39.11	67.8	3.60	5.34	5.13

MeV D-T neutrons which in turn interact with the sphere and target materials and generate gamma photons.

The photon leakage from the outer surface of the spherical samples is measured in the energy range 0.37 MeV–8.16 MeV by a scintillation detector (stilbene crystal of diameter 60 mm and height 60 mm) located 8.5 m away from the center of the sphere. The stilbene crystal was adopted because the scintillation pulse shape offers excellent neutron-photon discrimination and its own neutron activation does not perturb the results. One downside of the stilbene crystal is its relatively poor energy resolution, in the range 15–20% for energies <0.5 MeV, about 10% for ^{60}Co lines (1.17 and 1.33 MeV) and about 6–7% for energies > 3 MeV. The unfolding process from the electron-recoil spectra of the detector to the photon spectra in the energy domain was conducted using a mathematical method of "generalized differentiation" described in Ref. [19].

The total uncertainty in the absolute values of measured photon spectra is estimated at around 12%, accounting for several sources of uncertainty that are assumed to be uncorrelated: statistical uncertainty in the detector counting (about 5%) and efficiency (about 8%), uncertainty in the mathematical processing of the experimental spectra (about 7%) and uncertainty in the sphere radii and size of the tritium target. This 12% uncertainty is assumed at three standard deviations (3σ).

In addition to photon measurements, the NEA-1517/74 benchmark contains total neutron leakage measurements for the seven spheres (Al, Ti, Fe, Cu, Zr, Pb and ^{238}U). The data, which is incorrectly presented as photon flux leakage in Ref. [4], is reproduced in Table 2. Absolute measurements of the neutron flux in the installation were conducted with aluminum dosimeters exploiting the reaction ^{27}Al(n,α)^{24}Na and applied to calibrate an all-wave detector. The values in Table 2 were then measured experimentally as a relationship of the count rate of the all-wave detector with and without the spherical sample. Other neutron leakage measurement data obtained with a stilbene detector (diameter = height = 70 mm) is available in Ref. [11].

3.2. Review

The content of the benchmark documentation is reviewed in this section. We first tackle the data concerning the geometry of the

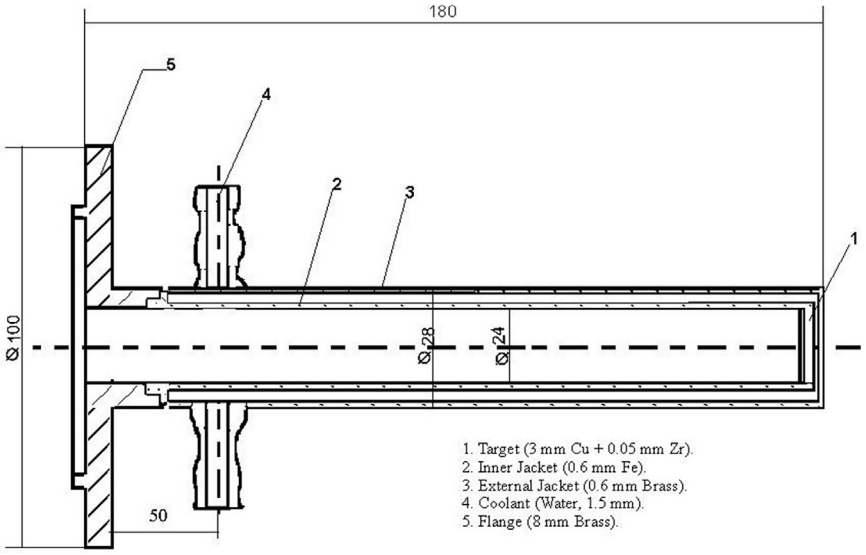

Fig. 2. Design of the target unit (dimensions in mm) [4].

Table 2
Total neutron leakage (number of neutrons) from spherical samples per neutron source.

Al	Ti	Fe	Cu	Zr	Pb	^{238}U
0.94	1.06	1.06	1.15	1.20	1.30	2.15

experimental room. The available benchmark documentation from SINBAD provides no information about: 1) the geometry and materials of the scintillation detector, apart from its stilbene crystal; 2) the distance and relative position of the lead bricks (detector shield) to the detector; 3) the distance of the neutron source to the steel rod, to the polyethylene collimator and to the concrete wall; 4) the inner diameter of the polyethylene collimator and the dimensions of the wall hole and wall collimators; 5) the geometry and relative position of the tube-holder pedestal behind the spherical sample. Contradictory information is given on the length of the concrete wall: 160 cm as shown in Fig. 1 but 150 cm as written in Refs. [4,5]. This lack of information severely limits the possibility of modelling in details the experimental room. Reference [4] provides one single MCNP input (iron sphere case) modelling only a perfect iron sphere. Reference [5] provides one single MCNP input (water sphere case) which only models the spherical sample, the target unit and the 40-cm long steel rod (its ends are modelled 15 cm and 55 cm away from the neutron source), with a point detector located 8.5 m away from the neutron source in the direction of the steel rod.

The geometry and materials of the spherical sample with its target unit are now addressed. The exact composition of the brass (% of copper and zinc) in Fig. 2 is not indicated. In general, no information about the impurities in materials (sample materials, steel, target unit materials, etc.) is provided. For the spherical samples made of loose materials, the thickness of the iron container is reported as 0.5 mm in Ref. [11] but modelled as 0.4 mm in the MCNP input of [5].

The benchmark does not give information about the angular and energy distribution of the D-T neutron source. Instead, it is suggested to model the neutron source as an isotropic monokinetic point source of energy 14.04981 MeV (energy released in D-T reaction multiplied by the ratio of helium nuclide mass to neutron and helium nuclide masses). According to the authors of the benchmark, these simplifications can affect the interpretation of the neutron measurements but are insignificant for photon measurements [5]. The experimental uncertainty of the total neutron leakage measurement of Table 2 is not indicated in the benchmark.

Finally, it must be mentioned that the RFNC experiments have been conducted for both spherical and hemispherical samples: Refs. [4,5] provide experimental leakage flux data for hemispherical sample measurements. However, no description on the exact orientation of the hemispheres relatively to the neutron source or the detector is provided in the benchmark documentation. Also, by nature of the experiment, the background noise is expected to be higher for the hemisphere measurements than for the sphere measurements (more neutron leakage and parasitic neutron captures) and the effect of neutron scattering on the structural materials of the experimental room is expected to be stronger. In the absence of data regarding the relative position of elements in the experimental room and the orientation of the hemisphere, we make the choice to disregard the hemisphere measurement data and to only focus on the sphere measurement data.

3.3. MCS model

The MCS inputs model the ten spherical samples with the target unit, beam tube and cooling water circuit. The iron container (0.4 mm thick) is modelled for the three loose sample materials. MCS and MCNP inputs are provided as supplementary material and the MCS input for a sphere of loose sample material with iron containers is illustrated in Fig. 3.

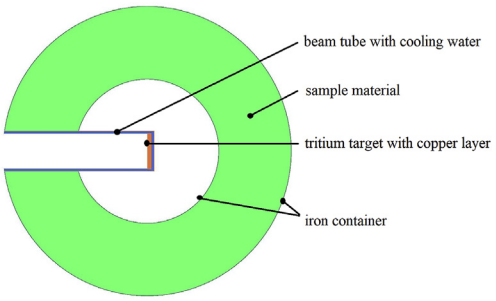

Fig. 3. MCS model of the spherical sample with beam tube, cooling water, tritium target and iron containers.

The weights presented in Table 1 are assumed to be the weights of the material sample only (i.e. it does not include the weights of the target unit and iron container) and the modelled densities of the sample materials are adjusted to match those weights. The

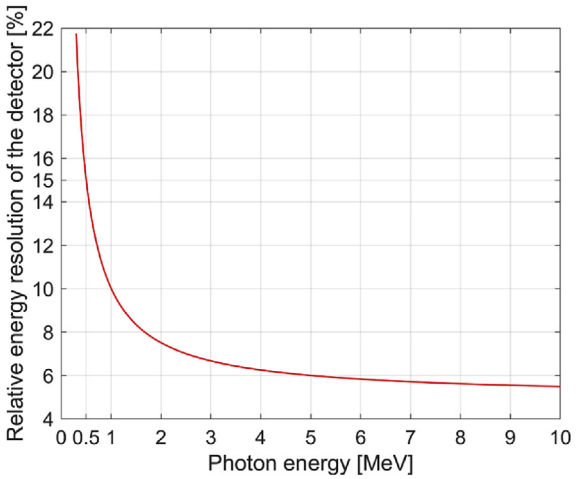

Fig. 4. Modelled energy resolution of the photon detector in the Monte Carlo simulations.

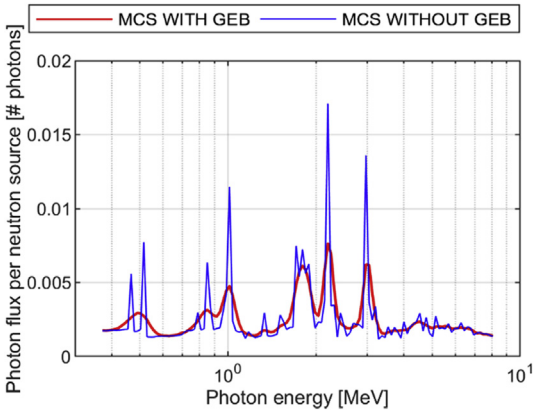

Fig. 5. Leakage photon flux from the aluminum sphere tallied with and without Gaussian energy broadening.

brass is approximated as 100% copper and 100% ^{238}U composition is adopted for the depleted uranium sphere. We expect the effect of material impurities on the photon leakage spectra to be negligible and the materials are modelled according to the natural abundances of their elements.

An isotropic monokinetic point neutron source of energy 14.04981 MeV is modelled at the center of the spherical samples. All the calculations are conducted in neutron-photon transport mode and 40 million neutron source histories are employed per calculation. The neutron and photon flux leaking out of the sphere is tallied in the volume between the spheres of radius R = 849 cm and R = 851 cm. This tallied flux in unit 1/cm^2 is then multiplied by the surface of the sphere of radius R = 850 cm to yield the leakage flux in unit number of particles (# particles), which can be compared directly to the experimental data.

The energy resolution of the stilbene-crystal scintillation

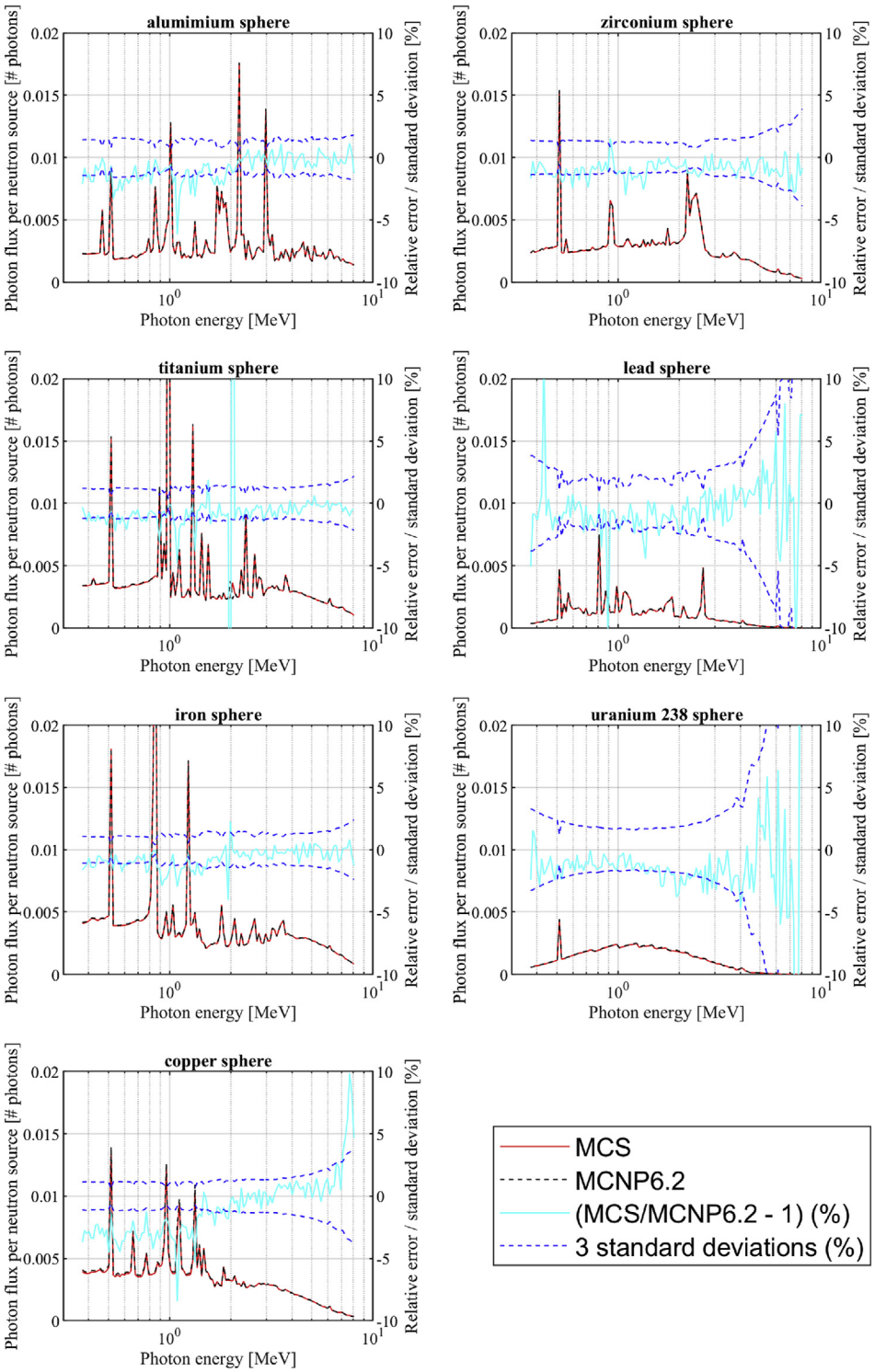

Fig. 6. NEA-1517/74: ENDF/B-VII.1 photon leakage flux without GEB of MCS vs MCNP6.2.

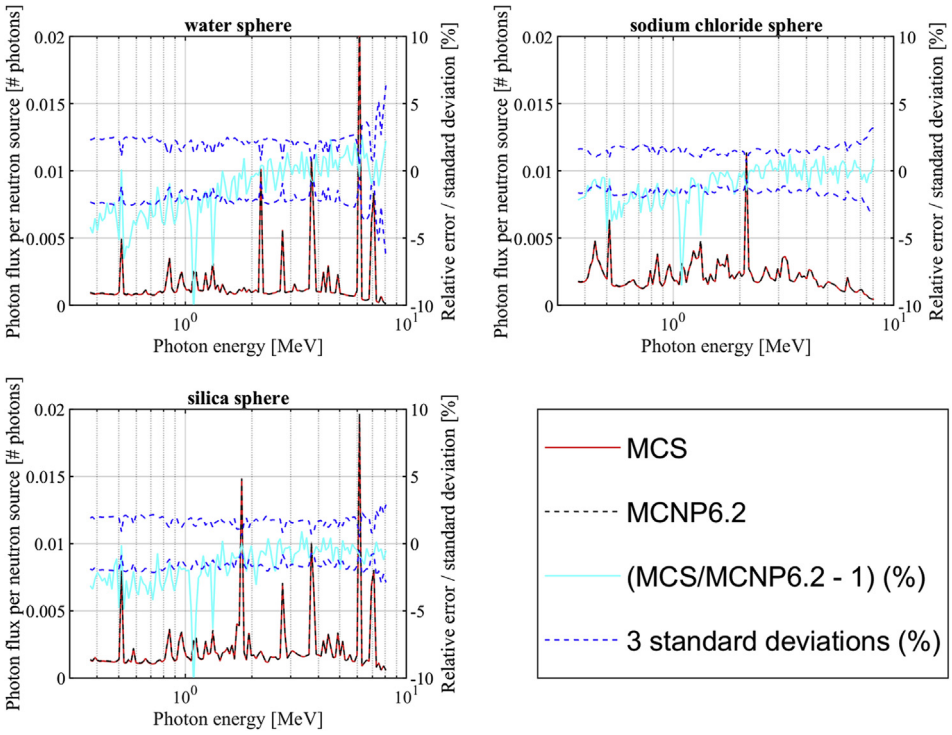

Fig. 7. NEA-1517/80: ENDF/B-VII.1 photon leakage flux without GEB of MCS vs MCNP6.2.

detector causes the experimental photon peaks to be lower in height and larger in width (broadening of the photon peaks). In order to model this effect in the Monte Carlo simulation, and thus to enable relevant comparisons of the calculated photon flux with the experimental benchmark data, Gaussian energy broadening (GEB) of the photon flux tally is applied during MCS calculations. For a photon of energy E, the GEB is applied with an energy-dependent full width at half maximum FWHM(E) given by Eq. (1) with A = 0.05 MeV, B = 0.005 $MeV^{1/2}$ and C = 100 MeV^{-1}. The relative energy resolution FWHM(E)/E modelled by this GEB is plotted as a function of the photon energy E in Fig. 4. It can be checked that this modelling of the FWHM matches well the energy resolution of the stilbene-crystal scintillation detector that is specified in the benchmark documentation, i.e. 15–20% below 0.5 MeV, 10% close to 1 MeV and 6–7% above 3 MeV. The effect of applying the GEB on the tallied photon leakage flux is illustrated for the aluminum sphere case in Fig. 5: just like experimental photon peaks, the photon peaks in the tallied photon spectrum become smaller and wider when applying the GEB, which is the intended effect.

$$\mathrm{FWHM}(E) = A + B\sqrt{E + C.E^2} \quad (1)$$

4. Results

4.1. Preliminary verification

A preliminary verification of the coupled neutron-photon transport of MCS is first carried out against the Monte Carlo code MCNP6.2 for the ten sphere cases with the library ENDF/B-VII.1. For this verification, the Gaussian energy broadening of the photon tallies is turned off as it is only needed for the comparison of calculated flux to experimental flux. The comparison results for the seven spheres of the NEA-1517/74 benchmark and the three spheres of the NEA-1517/80 benchmark are presented in Fig. 6 and Fig. 7 respectively. A good agreement is observed within 5% or three standard deviations for the calculated photon leakage flux between MCS and MCNP6.2, thus verifying the capability of MCS to conduct the neutron-photon interpretation of the RFNC benchmark.

4.2. Sensitivity tests

The necessity to model the target unit inside the spherical sphere, including the beam tube, tritium target and cooling water circuit, is highlighted. The calculations of photon leakage are performed for the seven spheres of the NEA-1517/74 benchmark with a perfect hollow sphere of inner radius 5 cm and outer radius 10 cm without the target unit (simple sphere model). Those calculations with the simple sphere model are compared to calculations with the more detailed sphere model of Fig. 3 (complex sphere model). The ENDF/B-VII.1 library is used in this comparison. Gaussian energy broadening is not applied. Table 3 summarizes the calculated number of leakage photons per neutron source with the simple and complex sphere models (statistical uncertainty at one standard deviation is about 0.1%). For all the spheres except ^{238}U, modelling the target unit leads to a significant increase in the photon leakage

Table 3
NEA-1517/74: MCS & ENDF/B-VII.1 number of leakage photons per neutron source for the simple and complex sphere models.

Sphere material (density in g/cm^3)	Simple sphere (S)	Complex sphere (C)	S/C-1
Al (2.71)	0.4165	0.5102	−18.4%
Ti (4.45)	0.5613	0.6228	−9.9%
Zr (6.51)	0.3468	0.3866	−10.3%
Fe (7.40)	0.5977	0.6249	−4.4%
Cu (8.23)	0.5081	0.5354	−5.1%
Pb (10.76)	0.1286	0.1379	−6.8%
^{238}U (18.66)	0.1720	0.1693	+1.6%

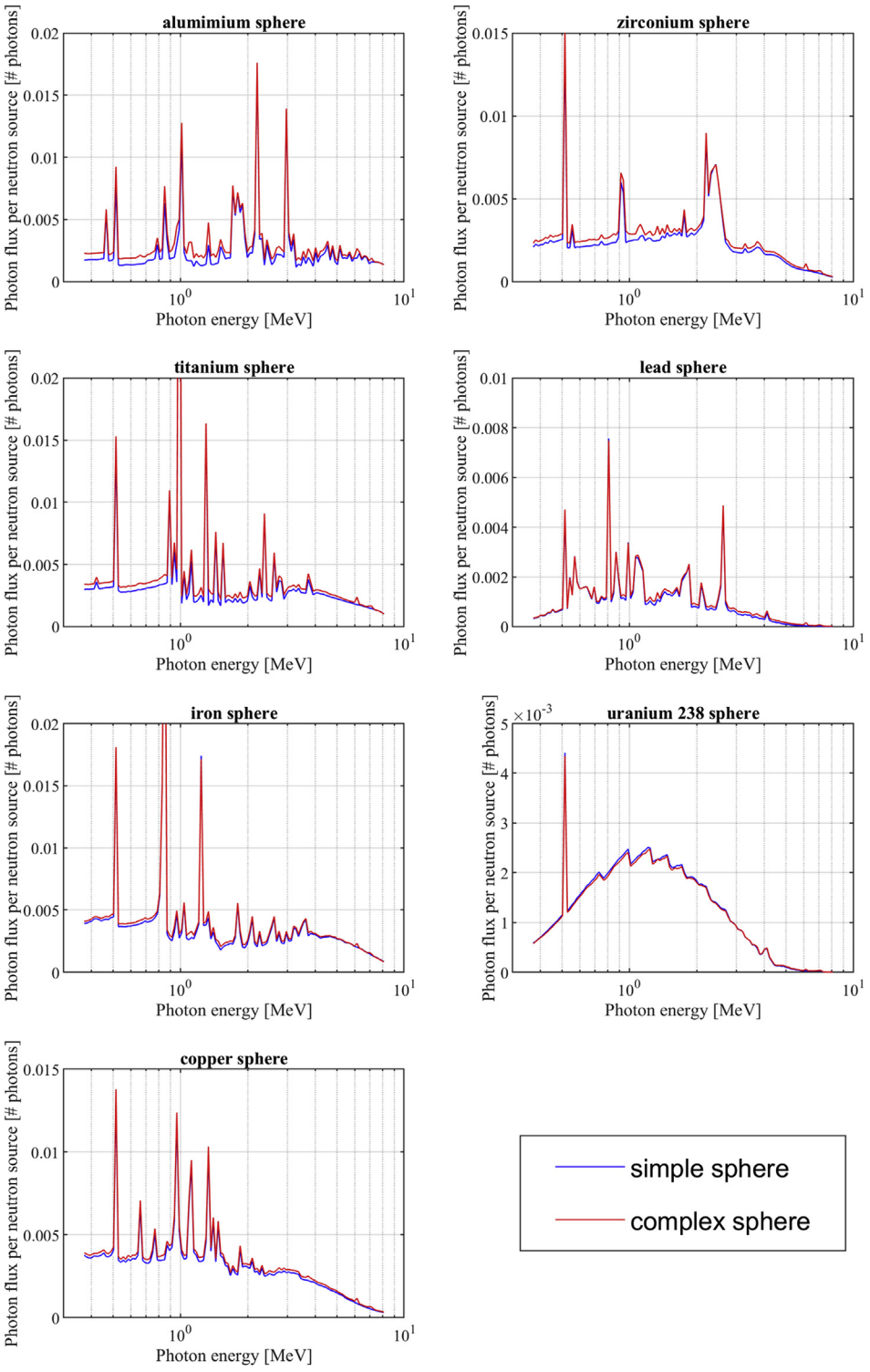

Fig. 8. NEA-1517/74: MCS & ENDF/B-VII.1 photon leakage flux without GEB for the simple and complex sphere models.

flux. The presence of the steel inner jacket, cooling water and copper external jacket of the beam tube in the complex model mechanically leads to neutron captures and additional gamma production in those materials compared to the simple model. The lighter the spherical sample material, the more those extra gamma photons produced inside the complex sphere can transmit through the sphere material and increase the photon leakage compared to the simple sphere model, as can be seen in Table 3 where the sphere materials are sorted by increasing densities. For the uranium sphere, it is observed that the gamma production in the uranium material decreases by about 2% in the complex sphere model compared to the simple model while the extra gamma photons produced in the target unit of the complex model are nearly all shielded by the 5-cm thickness of depleted uranium. This

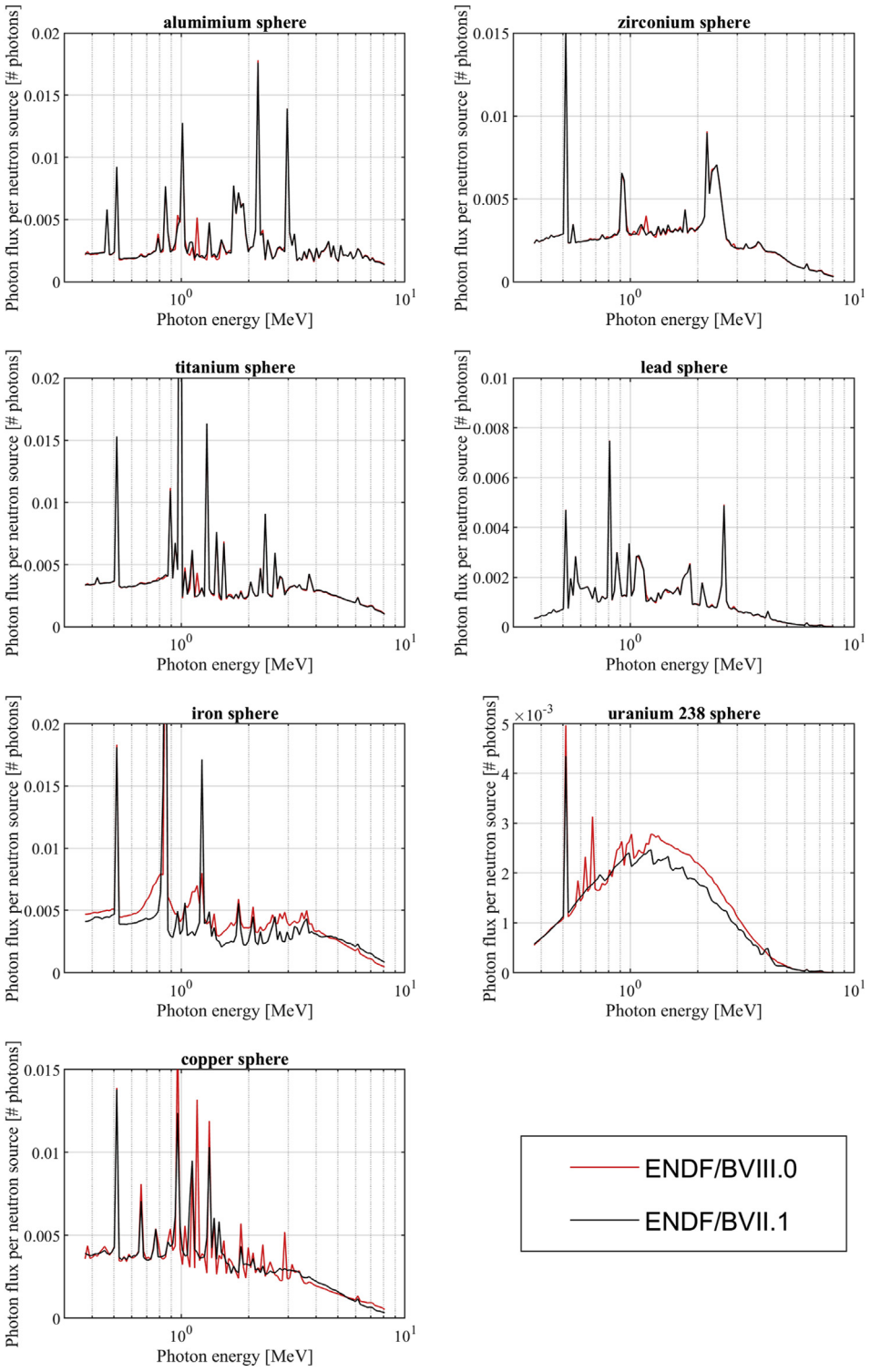

Fig. 9. NEA-1517/74: MCS photon leakage flux without GEB with the libraries ENDF/B-VII.1 and B-VIII.0.

effect for the uranium sphere case leads in total to a decrease of the photon leakage in the complex model compared to the simple model. The photon leakage flux for the simple and complex sphere models are plotted in Fig. 8 for the seven spheres of NEA-1517/74 benchmark.

The photon leakage flux calculated for the complex sphere model with the libraries ENDF/B-VII.1 and ENDF/B-VIII.0 are compared for the seven spheres of the NEA-1517/74 benchmark and the three spheres of the NEA-1517/80 benchmark in Fig. 9 and Fig. 10 respectively (Gaussian energy broadening is not applied on the photon tallies). The total number of leakage photons per neutron source for each sphere case and each library is summarized in Table 4. The effect of the library update for the iron and copper isotopes (new neutron cross sections) and uranium 238 (new

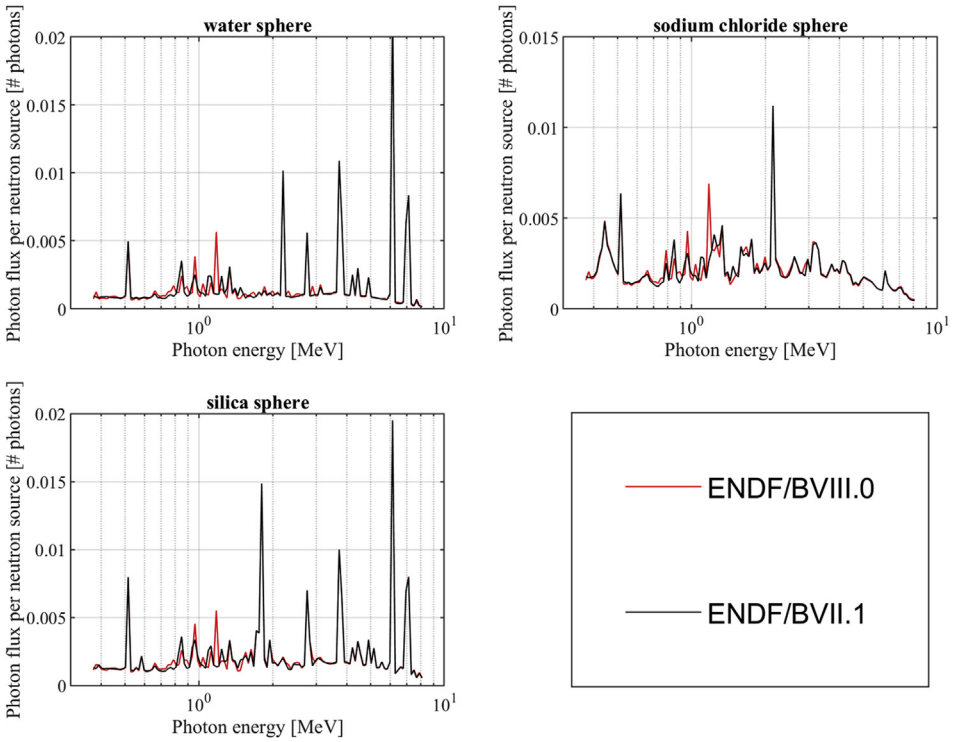

Fig. 10. NEA-1517/80: MCS photon leakage flux without GEB with the libraries ENDF/B-VII.1 and B-VIII.0.

Table 4
NEA-1517/74 & 80: MCS number of leakage photons per neutron source for the libraries ENDF/B-VII.1 & B-VIII.0.

	ENDF/B-VII.1 (B71)	ENDF/B-VIII.0 (B80)	(B71/B80-1) ± 0.2% (3σ)
Al	0.5102	0.5070	+0.7%
Ti	0.6228	0.6228	0.0%
Fe	0.6249	0.7068	−11.6%
Cu	0.5354	0.5405	−1.0%
Zr	0.3866	0.3873	−0.2%
Pb	0.1379	0.1383	−0.3%
^{238}U	0.1693	0.1855	−8.7%
H_2O	0.2540	0.2521	+0.8%
SiO_2	0.3514	0.3498	+0.5%
NaCl	0.3435	0.3428	+0.2%

Table 6
NEA-1517/74 & 80: number of leakage photons with GEB in the measured range 0.3679–8.159 MeV per neutron source.

	MCS + ENDF/B-VIII.0	Experimental data (EXP ± 12% at 3σ)	MCS/EXP-1
Al	0.3755	0.3888	−3.4%
Ti	0.4747	0.4377	+8.5%
Fe	0.5456	0.4372	+24.8%
Cu	0.4236	0.4717	−10.2%
Zr	0.3383	0.3194	+5.9%
Pb	0.1323	0.1212	9.2%
^{238}U	0.1742	0.1438	+21.1%
H_2O	0.2032	0.1894	+7.3%
SiO_2	0.2790	0.2821	−1.1%
NaCl	0.2730	0.2215	+23.2%

prompt fission gamma spectrum) is particularly visible, with an total increase of the photon leakage flux by 11.6% for the iron sphere, 8.7% for the uranium 238 sphere and 1.0% for the copper sphere. No relevant changes between the two libraries were noted for the isotopes of zirconium, titanium and lead and the photon leakage spectra for those spheres are essentially the same, the small differences being due to the copper and iron materials of the target unit inside the sphere. Differences for the leakage spectra of the aluminum, water, silica and sodium chloride spheres can be explained by the structural materials (0.4 mm thickness of iron on the internal and external surfaces of the spheres containing loose materials) and the additional gamma lines introduced in the library ENDF/B-VIII.0 for ^{27}Al, ^{23}Na, ^{28}Si and ^{35,37}Cl.

4.3. Experimental validation

The total neutron leakage per neutron source calculated by MCS with the ENDF/B-VIII.0 library is first compared in Table 5 against the experimental data (only available for the seven spheres of NEA-1517/74 benchmark). The statistical uncertainty of the calculated values is negligible (<0.1%). An agreement within 4% is observed between calculation and experiment, which is fair given that the experimental uncertainties of the neutron leakage values in Table 5

Table 5
NEA-1517/74: comparison of total neutron leakage between MCS + ENDF/B-VIII.0 and experimental data.

	Al	Ti	Fe	Cu	Zr	Pb	^{238}U
Experimental data (E)	0.94	1.06	1.06	1.15	1.20	1.30	2.15
MCS + ENDF/B-VIII.0 (C)	0.959	1.076	1.099	1.132	1.170	1.290	2.101
C/E − 1	+2.0%	+1.5%	+3.7%	-1.6%	-2.5%	-0.8%	-2.3%

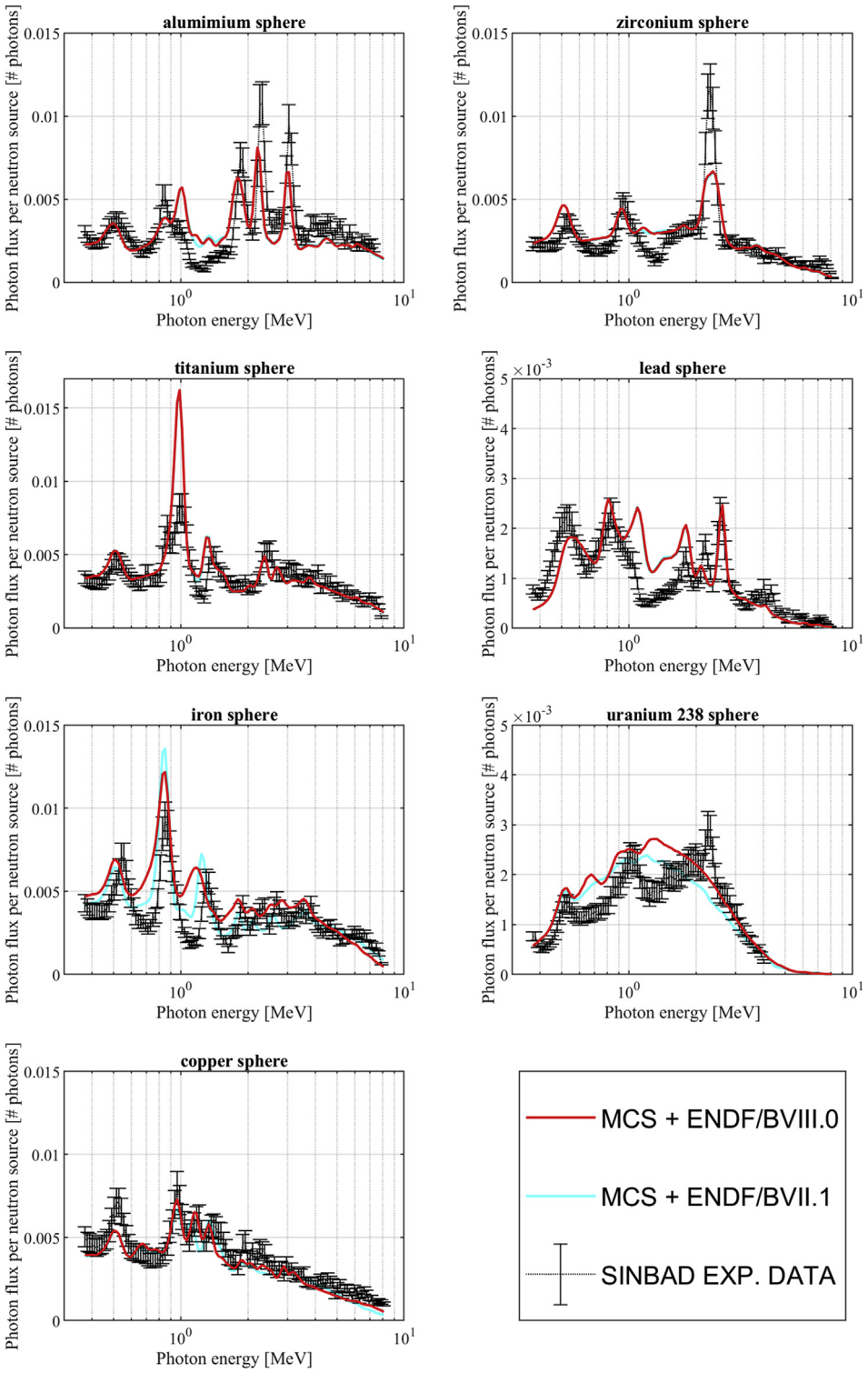

Fig. 11. NEA-1517/74: MCS photon leakage flux with GEB versus experimental data.

are not known and that the MCS model uses a simple isotropic monokinetic neutron source at the center of the sphere. The photon leakage in the measured energy range (0.3679 MeV–8.159 MeV) calculated by MCS with the ENDF/B-VIII.0 library and Gaussian energy broadening is then compared against the experimental photon leakage data in Table 6. The statistical uncertainty of the calculated values is negligible (<0.1%). Three spheres fall out of the 12% experimental uncertainty at three standard deviations: iron (+24.8%), uranium 238 (+21.1%) and sodium chloride (+23.2%).

The detailed comparison of the photon leakage spectra calculated by MCS with Gaussian energy broadening versus the experimental data is displayed in Fig. 11 for the seven spheres of the NEA-1517/74 benchmark and in Fig. 12 for the three spheres of the NEA-1517/80 benchmark. The error bars plotted for the experimental

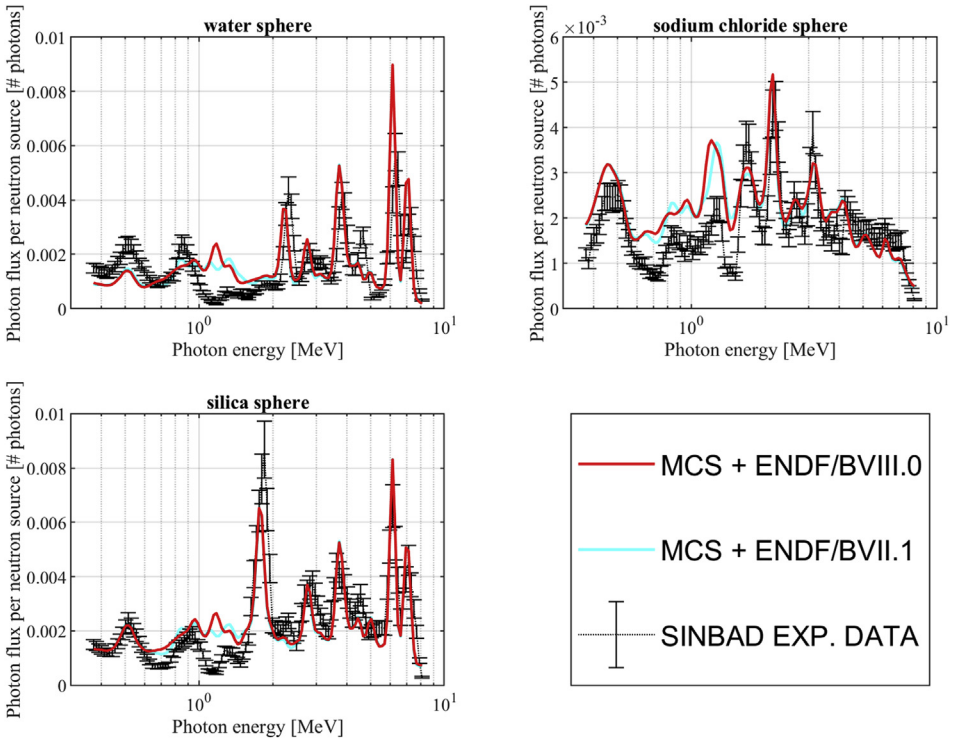

Fig. 12. NEA-1517/80: MCS photon leakage flux with GEB versus experimental data.

spectra correspond to a relative uncertainty of 12% (three standard deviations). The statistical uncertainties for the calculated flux are very small and correspond to the thickness of the lines. The results are commented element by element. For aluminum, the shapes of the calculated and experimental spectra are consistent. The experimental peaks close to 1.87 MeV, 2.3 MeV and 3 MeV are underestimated by about 20–30%. For titanium, the calculated and experimental spectra are in close agreement except for the experimental peak close to 1 MeV which is overestimated by nearly a factor of 2. For iron, a good agreement is observed and the height of the experimental gamma peak close to 840 keV is better calculated by the library ENDF/B-VIII.0 than by ENDF/B-VII.1. Excellent agreement is observed for the copper sphere although the 511 keV positron annihilation peak is underestimated by about 30%. For zirconium, the calculated and experimental spectra are in close agreement except for the experimental peak close to 2.3 MeV which is underestimated by a factor of 2. For lead, the agreement between calculated and experimental spectra is satisfying although the calculated spectrum displays a gamma peak close to 1 MeV which is absent in the experimental spectrum. For uranium 238, the spectrum calculated with ENDF/B-VIII.0 is globally higher than the spectrum calculated with ENDF/B-VII.1. Both calculated spectra seem to miss the experimental peak close to 2.3 MeV and the shapes of the calculated and experimental spectra are notably different in the range 600 keV to 2.5 MeV. It is worth noting that the original authors of the RFNC benchmark have claimed that the 2.3 MeV experimental peak for the uranium sphere case is probably related to the experimental configuration and they have suggested it could originate from the capture of slow neutrons by hydrogen in the concrete walls of the experimental room [4]. For the water sphere, the 511 keV positron annihilation peak is underestimated by about 40%, the experimental peak close to 6.3 MeV is overestimated by about 50% and the shapes of the spectra are different in the range 800 keV to 1.5 MeV. For the silica sphere, the shapes of the spectra are consistent but the experimental peak close to 1.8 MeV is underestimated by about 30%. Finally, for the sodium chloride sphere, excellent agreement is observed between the shapes of the experimental and calculated spectra, but the experimental spectrum is overestimated in the range 600 keV to 1.5 MeV.

5. Conclusions and perspectives

The interpretation of the experimental gamma leakage spectra from a spherical sample with a central D-T 14 MeV neutron source as described in the NEA-1517/74 and NEA-1517/80 benchmarks (RFNC benchmark) from the SINBAD database is conducted with the Monte Carlo code MCS developed at the Ulsan National Institute of Science and Technology, the photon library EPICS2014 and the most up-to-date ENDF/B-VIII.0 neutron library. The benchmark documentation describes satisfactorily the geometry of the sample sphere and the energy resolution of the photon detector but should ideally provide more information regarding the characteristics (energy – angle) of the neutron source, the geometry of the photon detector, the geometry of the experimental room (concrete walls) and the distances of shields and collimators relatively to the sample sphere.

A preliminary verification of MCS neutron-photon transport calculations against the Monte Carlo code MCNP6.2 shows a good agreement in the calculated photon leakage flux and confirms the suitability of MCS for the interpretation of the benchmark. A sensitivity study with and without modelling the target unit (beam tube, tritium target and cooling water) confirms the necessity to model the target unit inside the spherical sample, with a large impact on the total photon leakage (up to +18% for the aluminum sphere case). The impact of the update of gamma-production data between ENDF/B-VII.1 and ENDF/B-VIII.0 is assessed for the ten cases of the RFNC benchmark and notable differences are observed for the iron, copper and uranium-238 sphere cases. With the notable exception of the uranium-238 sphere case, consistency is overall observed between the shapes of the gamma leakage

calculated by MCS with the library ENDF/B-VIII.0 and the experimental data. For further analysis of the calculation/experiment discrepancies, more information about the experimental setup is required, especially the exact locations of collimators and concrete shielding wall relatively to the sample sphere and the geometry of the photon detector with its surrounding lead brick shield. Modelling the experimental room is expected to improve the calculation-experiment agreement for the uranium-238 sphere case, especially regarding the experimental 2.3 MeV peak that is absent in the calculations. Also, the benchmark does not provide information about the energy distribution and the anisotropy of the experimental D-T neutron source, which is approximated as monokinetic and isotropic in this study. Simulating the deuteron stream and the kinematics of the deuteron-tritium reaction in the target would constitute an improvement by capturing more accurately the energy and angular distribution of the experimental neutron source and would help for the interpretation of the RFNC neutron leakage measurements.

Declaration of competing interest

The authors declare that they have no known competing financial interests or personal relationships that could have appeared to influence the work reported in this paper.

Acknowledgements

This work was supported by the National Research Foundation of Korea (NRF) grant funded by the Korea government (MSIT). (No. NRF-2019M2D2A1A03058371).

Appendix A. Supplementary data

Supplementary data to this article can be found online at https://doi.org/10.1016/j.net.2019.12.014.

References

[1] D.A. Brown, M.B. Chadwick, R. Capote, et al., ENDF/B-VIII.0: the 8th major release of the nuclear reaction data library with CIELO-project cross sections, new standards and thermal scattering data, Nucl. Data Sheets 148 (2018) 1–142, https://doi.org/10.1016/j.nds.2018.02.001.

[2] I. Kodeli, A. Milocco, P. Ortego, et al., 20 years of SINBAD (shielding integral benchmark archive and database), Prog. Nucl. Sci. Technol. 4 (2014) 308–311, https://doi.org/10.15669/pnst.4.308.

[3] I. Kodeli, G. Zerovnik, A. Milocco, Examples of use of SINBAD database for nuclear data and code validation, EPJ Web Conf. 153 (2017), https://doi.org/10.1051/epjconf/201715302010, 02010.

[4] A.I. Saukov, V.D. Lyutov, E.N. Lipilina, et al., Photon Leakage Spectra from Al, Ti, Fe, Cu, Zr, Pb, U238 Spheres, 2006. OECD/NEA DB Computer Code, Package NEA-1517/74.

[5] A.I. Saukov, V.D. Lyutov, E.N. Lipilina, et al., RFNC Photon Spectra from H2O, SiO2 and NaCl, 2007. OECD/NEA DB Computer Code, Package NEA-1517/80.

[6] A. Serikov, U. Fischer, D. Leichtle, et al., Monte Carlo radiation shielding and activation analyses for the diagnostic equatorial port plug in ITER, Fusion Eng. Des. 87 (2012) 690–694, https://doi.org/10.1016/j.fusengdes.2012.02.003.

[7] M. Lemaire, C. Vaglio-Gaudard, A. Lyoussi, et al., For a better estimation of gamma heating in nuclear material-testing reactors and associated devices: status and work plan from calculation methods to nuclear data, J. Nucl. Sci. Technol. 52 (9) (2015) 1093–1101, https://doi.org/10.1080/00223131.2015.1009957.

[8] M. Lemaire, C. Vaglio-Gaudard, A. Lyoussi, et al., Experimental validation of photon-heating calculation for the Jules Horowitz reactor, Nucl. Instrum. Methods Phys. Res. Sect. A Accel. Spectrom. Detect. Assoc. Equip. 780 (2015) 68–80, https://doi.org/10.1016/j.nima.2015.01.054.

[9] P. Blaise, J. Di Salvo, C. Vaglio-Gaudard, et al., Nuclear heating measurement in critical facilities and experimental validation of code and libraries - an application to prompt and delayed γ nuclear data needs, Phys. Procedia 59 (2014) 3–16, https://doi.org/10.1016/j.phpro.2014.10.002.

[10] C. Liegeard, A. Calloo, G. Marleau, et al., Impact of photon transport on power distribution, in: Proc. Int. Conf. M&C, Korean Nuclear Society, 2017. Jeju, South Korea, Apr 16-20 (2017).

[11] A.I. Saukov, E.N. Lipilina, V.D. Lyutov, Measurements of neutron and photon leakage from spherical and hemispherical samples with a central 14-MeV neutron source as a possible type of benchmarks, in: Proc. Int. Conf. ICRS10–RPS2004, 2004, pp. May 9–14. Madeira, Portugal.

[12] B. Colling, I. Kodeli, S. Lilley, et al., Benchmarking comparison and validation of MCNP photon interaction data, EPJ Web Conf. 146 (2017), https://doi.org/10.1051/epjconf/201714606024, 06024.

[13] D.H. Lee, J.S. Kim, S.K. Lim, et al., McCARD gamma transport analysis for RFNC photon spectrum benchmark, in: Proc. Int. Conf. KNS Autumn Meeting, 2018. Yeosu, South Korea, October 24-26.

[14] J. Jang, W. Kim, S. Jeong, et al., Validation of UNIST Monte Carlo code MCS for criticality safety analysis of PWR spent fuel pool and storage cask, Ann. Nucl. Energy 114 (2018) 495–509, https://doi.org/10.1016/j.anucene.2017.12.054.

[15] H. Lee, W. Kim, P. Zhang, et al., MCS – a Monte Carlo particle transport code for large-scale power reactor analysis, Ann. Nucl. Energy 139 (2020), 107276, https://doi.org/10.1016/j.anucene.2019.107276.

[16] M. Lemaire, H. Lee, B. Ebiwonjumi, et al., Verification of photon transport capability of UNIST Monte Carlo code MCS, Comput. Phys. Commun. 231 (2018) 1–18, https://doi.org/10.1016/j.cpc.2018.05.008.

[17] R.E. MacFarlane, A.C. Kahler, Methods for processing ENDF/B-VII with NJOY, Nucl. Data Sheets 111 (2010) 2739–2890, https://doi.org/10.1016/j.nds.2010.11.001.

[18] S.C. van der Marck, Benchmarking ENDF/B-VII.1, JENDL-4.0 and JEFF-3.1.1 with MCNP6, Nucl. Data Sheets 113 (2012) 2935–3005, https://doi.org/10.1016/j.nds.2012.11.003.

[19] A.I. Saukov, B.I. Sukhanov, A.M. Ryabinin, et al., Photon leakage from spherical and hemispherical samples with a central 14-MeV neutron source, Nucl. Sci. Eng. 142 (2002) 158–164, https://doi.org/10.13182/NSE02-A2296.